Research Article

Photocatalytical Antibacterial Activity of Mixed-Phase TiO$_2$ Nanocomposite Thin Films against *Aggregatibacter actinomycetemcomitans*

Sinem Yeniyol,[1] Ilven Mutlu,[2] Zhiming He,[3] Behiye Yüksel,[4] Robert Joseph Boylan,[3] Mustafa Ürgen,[5] Zihni Cüneyt Karabuda,[1] Cansu Basegmez,[1] and John Lawrence Ricci[6]

[1]*Department of Oral Implantology, Faculty of Dentistry, Istanbul University, 34093 Istanbul, Turkey*
[2]*Metallurgical and Materials Engineering Department, Faculty of Engineering, Istanbul University, Avcilar, 34320 Istanbul, Turkey*
[3]*Department of Basic Science and Craniofacial Biology, New York University College of Dentistry, New York, NY 10010, USA*
[4]*Department of Mechanical Engineering, Istanbul Aydın University, 34668 Istanbul, Turkey*
[5]*Department of Metallurgical and Materials Engineering, Faculty of Chemical and Metallurgical Engineering, Istanbul Technical University, 34469 Istanbul, Turkey*
[6]*Department of Biomaterials and Biomimetics, New York University College of Dentistry, New York, NY 10010, USA*

Correspondence should be addressed to Sinem Yeniyol; yeniyols@istanbul.edu.tr

Mixed-phase TiO$_2$ nanocomposite thin films consisting of anatase and rutile prepared on commercially pure Ti sheets via the electrochemical anodization and annealing treatments were investigated in terms of their photocatalytic activity for antibacterial use around dental implants. The resulting films were characterized by scanning electron microscopy (SEM), and X-ray diffraction (XRD). The topology was assessed by White Light Optical Profiling (WLOP) in the Vertical Scanning Interferometer (VSI) mode. Representative height descriptive parameters of roughness R_a and R_z were calculated. The photocatalytic activity of the resulting TiO$_2$ films was evaluated by the photodegradation of Rhodamine B (RhB) dye solution. The antibacterial ability of the photocatalyst was examined by *Aggregatibacter actinomycetemcomitans* suspensions in a colony-forming assay. XRD showed that anatase/rutile mixed-phase TiO$_2$ thin films were predominantly in anatase and rutile that were 54.6 wt% and 41.9 wt%, respectively. Craters (2–5 μm) and protruding hills (10–50 μm) on Ti substrates were produced after electrochemical anodization with higher R_a and R_z surface roughness values. Anatase/rutile mixed-phase TiO$_2$ thin films showed 26% photocatalytic decolorization toward RhB dye solution. The number of colonizing bacteria on anatase/rutile mixed-phase TiO$_2$ thin films was decreased significantly *in vitro*. The photocatalyst was effective against *A. actinomycetemcomitans* colonization.

1. Introduction

Since the discovery of the photocatalytic oxidation for water on titanium dioxide (TiO$_2$) electrode in 1972 by Fujishima and Honda [1], TiO$_2$ is believed to be the most promising photocatalyst owing to its superior photoreactivity, nontoxicity, chemical stability, low price, and repeated use without substantial loss of catalytic activity [2–4]. Photocatalytic water splitting has been the focus of interest for TiO$_2$-based photochemistry [5]. The fundamental mechanism underlying the photocatalytic killing has not been well established yet [6].

The photocatalytic activity of TiO$_2$ is significantly influenced by various parameters including crystalline structure, impurities, surface area, and density of surface hydroxyl groups [7]. However, the most significant factor is its crystalline structure. TiO$_2$ is usually used as a photocatalyst in two crystal structures: rutile and anatase. Anatase generally has a larger band gap (3.2 eV) than rutile (3.0 eV) with much higher photocatalytic activity [2]. The generation of electron-hole pairs is detrimental to this photocatalytic efficiency of the photocatalyst. Upon excitation by light with energy equal to or higher than the band gap energy, the photon energy

generates electrons excited from the valence band to the conduction band and holes at the valance band on the TiO$_2$ surface. The hole in the valance band can react with H$_2$O or hydroxide ions adsorbed on the surface to produce hydroxyl radicals, and the electron in the conduction band can reduce O$_2$ to produce superoxide ions (O$_2^-$). Both holes and OH$^-$ are extremely reactive with contacting organic compounds [6, 8]. It was stated that these crystalline phases of TiO$_2$, consisting of mixed rutile and anatase with an appropriate ratio, enhanced the photocatalytic properties [9]. For this reason, many studies commonly used the conventional mixed-phase photocatalyst powder Degussa P25 (Degussa Chemical Company, Teterboro, New Jersey, USA) consisting of anatase 80% and rutile 20% [2, 6, 10]. However, continuously stirring during the reaction process and their separation and recovery after reaction are their disadvantages. Recently, the use of immobilized thin TiO$_2$ film coatings on substrates forming photocatalytical surfaces makes it possible to overcome these disadvantages [6, 11]. Studies have been focused on the development of immobilized TiO$_2$ photocatalysts for their oxidative degradation of organic compounds as well as microorganisms [4]. Anatase/rutile mixed-phase TiO$_2$ were synthesized by various methods including sol-gel method [12], sputtering [13], chemical vapour deposition [14, 15], atomic layer deposition [16], plasma immersion ion implantation [17], cathodic arc deposition [18], and anodization [19]. Among these methods, anodization is a cost-effective and simple technique that allows controlled anatase/rutile mixed-phase TiO$_2$ formation on the substrates by means of altering the experimental conditions. To induce the TiO$_2$ phases, generally an annealing treatment of as-prepared film at above 450°C is necessary.

Various photocatalytic activity studies have been conducted to develop antibacterial effect. Most of the studies have tested the photocatalytic activity on *E. coli* [2, 6, 20]. Kim et al. [21] have used food-borne pathogenic bacteria, *S. choleraesuis* subsp., *V. parahaemolyticus*, and *L. monocytogenes*, and established a batch type photocatalytic reactor in order to investigate the bactericidal effect with various near-ultraviolet (UV) irradiation time and TiO$_2$ concentrations. Lee et al. [22] had modified a defense mechanism to nullify *B. anthracis* in case of a probable microbial attack using the photocatalyst technology. The antibacterial efficiency of long wave UV-irradiated TiO$_2$ thin films as well as the ultrastructural damage on bacterial cells was evaluated using *P. aeruginosa* as a model by Amézaga-Madrid et al. [23]. The most common and significant complication of dental implants is peri-implantitis which is closely related to the colonization of peri-implantitis-associated bacteria. Among these, *Aggregatibacter actinomycetemcomitans* is a gram-negative, nonmotile coccobacillus that colonizes the human oral cavity that jeopardizes the host's defense mechanism leading to peri-implantitis [24]. It is therefore most important to develop implant surfaces with antibacterial properties for maintaining plaque-free surfaces on titanium dental implants' transmucosal components exposed to the oral cavity. With the use of an appropriate anodization technique, universal control of the required surface properties resulting in reproducible photocatalytic anatase/rutile mixed-phase

TiO$_2$ thin films on almost any transmucosal component of a dental implant with antibacterial properties can be developed.

The present study is therefore designed to develop anatase/rutile mixed-phase TiO$_2$ thin films by electrochemical anodization and annealing treatments in order to investigate their influence on the photocatalytic degradation of RhB dye solution and the colonization of peri-implantitis-associated bacteria *Aggregatibacter actinomycetemcomitans* as an index of antibacterial photocatalytic activity *in vitro*.

2. Materials and Methods

2.1. Preparation of Samples. Commercially pure titanium (cpTi) (ASTM B265-02) sheets in squares (10 × 10 × 1 mm) were used as substrates for the experiments. The surfaces of the specimens were prepared by standard metallographical techniques. These sheets were ultrasonically cleaned in acetone, distilled water, and methanol, respectively. These untreated cpTi sheets were named as *Group Ti*. The electrochemical anodization was employed to form TiO$_2$ thin films on the cpTi sheets. Anodization voltage was performed under 40 V and each Ti surface (anode) was electrochemically anodized in 0.1 M KOH electrolyte for 3 minutes at 20°C [25]. Stainless steel was used as the counter electrode. In order to convert the amorphous TiO$_2$ thin films into the crystallized TiO$_2$ thin films, sheets were annealed at 550°C in air for 1 h after anodization treatment [26]. These sheets containing mixed-phase TiO$_2$ thin films consisting of anatase and rutile were named as *Group AR*.

2.2. Artificial Saliva Preparation. Artificial saliva solution was prepared from chemicals supplied by Merck, Germany [27, 28]. Amounts of reagents are 0.40 g/L NaCl, 0.79 g/L CaCl$_2$ H$_2$O, 0.40 g/L KCl, 0.005 g/L Na$_2$S 9H$_2$0, 0.78 g/L NaH$_2$PO$_4$ H$_2$O, and 0.35 g/L Urea-CO (NH$_2$). The pH of the artificial saliva solution was 6.30. The pH value of the artificial saliva solution was measured and monitored using a pH meter (WTW, InoLab 720, Germany).

2.3. Electrochemical Corrosion Study. Electrochemical corrosion studies were carried out in the artificial saliva solution using a potentiostat (Interface 1000 Potentiostat/Galvanostat/ZRA, Gamry Instruments Inc., USA) controlled by a personal computer. Volume of glass corrosion test cell was 1000 mL. A conventional three-electrode system with high-density graphite rod as a counter electrode, a saturated calomel electrode (SCE) as reference electrode, and specimen as a working electrode was used. Data acquisition was carried out through a computer software (Framework, Version 6.04, Gamry Instruments, USA), while data analysis was carried out by Echem Analyst Software, Version 6.04, Gamry Instruments, USA. Specimens were prepared by mounting into epoxy resin. So, only square sheet surface of the specimens was exposed to the artificial saliva solution. The specimens were connected to a copper wire. All experiments were carried out at room temperature.

Open circuit potential (OCP) of the specimens was measured before carrying out the electrochemical corrosion experiments. OCP level was measured for durations of 2 to 3 hours, until the OCP was stabilized.

Tafel curves were obtained by polarizing the specimens from −250 mV to +250 mV (versus SCE), with respect to the OCP, at scan rate of 1.0 mV/s. Tafel slopes were obtained from Tafel extrapolation analyses.

Cyclic polarization tests were carried out from −500 mV (versus SCE) to apex potential and to final potential, which was 0 mV (versus SCE). Forward and reverse polarization scan rates were 5 and 2.5 mV/s, respectively. Cyclic (forward and reverse) polarization technique was used to evaluate tendency to localized corrosion (pitting) in corrosive environment. Considerable hysteresis between the forward and reverse polarization sweeps is an indication of the pit formation.

2.4. Surface Characterization

2.4.1. White Light Interference Microscopy.
The surface topologies of the sheets were investigated with the White Light Optical Profiling (WLOP) Wyko-NT1100 (Veeco Instruments Inc., Plainview, NY, USA) at VSI (Vertical Scanning Interferometer) mode, which is a noncontact optical profiling system that provides high vertical resolution. Two height descriptive parameters of roughness as R_a and R_z were used to quantify the surface roughness, where R_a is the arithmetical mean roughness value from the profile mean along a defined sampling line, and R_z is named as ten-point mean roughness which is the mean of maximum peak-to-valley height of 5 consecutive sections of the sampling line.

2.4.2. Scanning Electron Microscopy.
The surface morphologies of the sheets were observed using a scanning electron microscope (SEM; JSM5410, JEOL, Tokyo, Japan) at a 10 kV acceleration voltage and magnifications of ×500 and ×3500.

2.4.3. X-Ray Diffraction.
The structure and phase of the Group Ti were monitored by utilizing a Philips PW 3710 grazing incidence X-ray diffractometer with a CuKα radiation (scan range 20° to 80°). A scan rate of 0.02°/sec was used with a grazing incidence of 0.5° for the Ti structure. The structure and phase of the Group AR were monitored by utilizing a Panalytical diffractometer (Phillips, Holland) using X-ray diffraction data collected in the reflection Bragg-Brentano geometry with a CuKα radiation under an applied voltage of 45 kV and a current of 40 mA. A scan rate of 0.03°/sec with a grazing incidence of 0.45° was used for the Ti and TiO$_2$ structure. The scanning data were recorded in the 2θ range of 20–73°. The phase contents of rutile and anatase (%W_A) and rutile (%W_R) for the anatase/rutile mixed-phase TiO$_2$ thin films at Group AR were estimated by utilizing the obtained patterns to determine weight percentage of the anatase phase and rutile phase TiO$_2$ using Spurr-Myers' equations [29] provided as in the following:

$$\%W_R = \frac{1}{1 + 0.884 \times \left(I_A/I_R\right)} \times 100,$$
$$\%W_A = \frac{1}{1 + 1.26 \times \left(I_R/I_A\right)} \times 100, \tag{1}$$

where I_R and I_A are the peaks areas in counts per second (c.p.s.) for the sharpest peaks for the (004) crystal plane of anatase TiO$_2$ and (110) crystal plane of rutile phase TiO$_2$, respectively. The numbers 0.884 and 1.26 are scattering coefficients [30, 31].

2.5. Photocatalytic Activity Evaluation.
The photoactivity of the anatase/rutile mixed-phase TiO$_2$ thin films was evaluated by studying their effect on the photodegradation of RhB dye solution (item # R6626, Sigma-Aldrich). RhB is a dye molecule, with a maximum absorption wavelength of 554 nm, that reacts with photogenerated oxyradicals and its loss may be monitored to evaluate the photocatalytic activity of the synthesized TiO$_2$ samples using a UV-visible spectroscopy. A 30 W UV lamp irradiating a wavelength of 254 nm was used as the irradiation source. Sheets were irradiated in the perpendicular direction at a distance of 2 cm measured from the UV source to the initial sample surface. 5 mL of aqueous RhB dye solution was placed in each chamber to carry out the experiments with a starting concentration of 0.5 mg/L. RhB dye solution was pipetted onto each of the glass chambers that contained sheets from both experimental groups. Empty glass chambers served as the controls in this photocatalytic activity evaluation assay and were named as *Group C*. The decomposition of RhB dye was monitored by measuring the absorbency at 554 nm (λmax) by a UV-visible (UV-Vis) spectrophotometer (Perken Elmer Lambda 9 Spectrometer), and the degradation rate (%) was evaluated by the following equation [32]:

$$D = \frac{C_t}{C_0} \times 100\%, \tag{2}$$

where D is degradation rate and C_0 and C_t are the concentrations of the RhB dye solution at UV irradiation times 0 and t, respectively. To compare the rate of RhB dye photodegradation, the absorption spectra of each sample were recorded at timed intervals, up to 2 h (15 min, 30 min, 45 min, 60 min, 75 min, 90 min, 105 min, and 120 min). All the experiments were conducted thrice, and mean values were used as the final result.

2.6. Colony-Forming Assay for Antibacterial Effect.
The tests were performed using *A. actinomycetemcomitans* (ATCC 43718; ATCC, Rockville MD, USA). Bacteria cells were cultured in brain heart infusion (BHI) broth (Thermo Scientific Remel, Lenexa, KS, USA) overnight at 37°C. Based on our pilot studies, the bacteria were grown to mid-log phase, centrifuged, and resuspended in trypticase soy broth to an optical density of approximately 0.40 at the wavelength

600 nm. Sheets from both experimental groups ($n = 78$ each) were placed into individual wells of the sterile 24-well culture plates with their modified surfaces placed facing upwards and bacteria cells were pipetted onto these sheets. Bacteria grown on culture plates' well bottoms were used as controls in this antibacterial assay and were named as *Group D* ($n = 78$). The culture plates were covered by their lids to prevent medium evaporation. Half of each group ($n = 36$ each) was exposed to UV irradiation (*as UV (+) condition*) (254 nm) while being incubated in an anaerobic environment (Modular Atmosphere Controlled System, DW Scientific, Shipley, Yorkshire, UK) at 37°C for 2 h, whereas the other halves ($n = 36$ each) were kept in a black box avoiding UV light penetration (*as UV (−) condition*) at the same experimental conditions. The supernatant fluid from each well was appropriately diluted and plated on TSBN media (personal communication, S. S. Socransky, Forsyth Institute, Cambridge, MA, USA) and incubated anaerobically for 4 days at 37°C and the number of colonies (colony-forming unit: CFU) was counted. TSBN was prepared as described elsewhere [33]. Antibacterial activity was expressed as the ratio of CFUs on each plate to those on the control group.

The power analysis was performed with PS Program (Power and Sample Size Program: http://biostat.mc .vanderbilt.edu/wiki/Main/PowerSampleSize) [34]. A *pre hoc* power analysis at 80% power, $\alpha = 0.05$, Δ: 1.1, and SD: 1.5, was performed, and it was determined that a minimum of 30 sheets in each group were necessary when comparing Group AR, Group Ti, and Group D.

2.7. Statistical Analysis. All data were analyzed with the statistical package for social sciences, 22.0 (SPSS for Windows; SPSS Inc., Chicago, Illinois, USA). The normality test of Shapiro-Wilks was applied and the data were found normally distributed. Interactions between parameters were defined using the two-way analysis of variance (ANOVA) followed by subsequent one-way ANOVA and Student's *t*-test. If one-way ANOVA suggested a significant difference between means among the groups, when equal variances could be assumed, *post hoc* testing was done using the Tukey HSD test; otherwise, Tamhane's $T2$ test for those with unequal variances was used. When the *p* value was less than 0.05, the statistical test was determined as significant. Data were expressed as mean ± standard deviation.

3. Results

3.1. Electrochemical Corrosion Study

3.1.1. Open Circuit Potential. Open circuit potential (OCP) is the potential at which an alloy is in equilibrium with the environment. High OCP value means that the material is stable in a certain corrosive environment. Figure 1 shows the variation of the OCP level in the Group AR and Group Ti specimens. As shown in Figure 1, Group AR specimen showed higher OCP values than the Group Ti specimen, which means Group AR specimen has higher corrosion resistance than the Group Ti specimen.
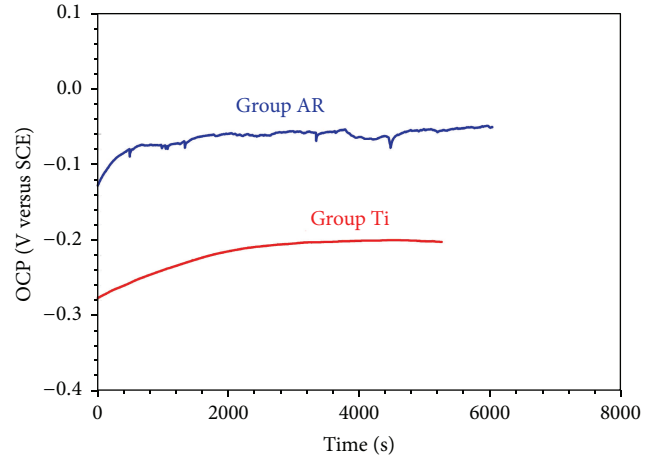

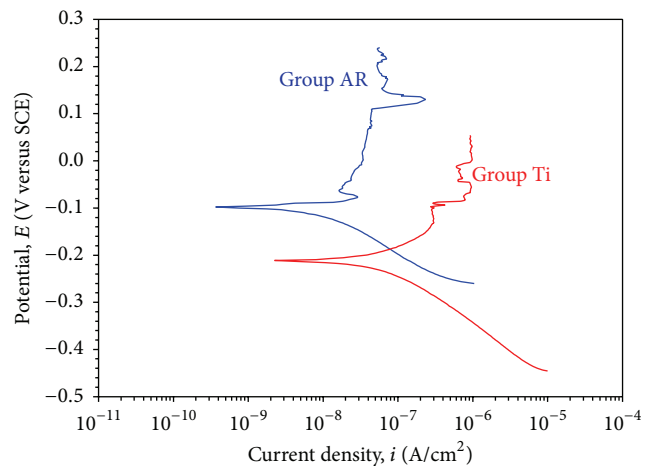FIGURE 1: Open circuit potential (OCP) curves of the Group AR and Group Ti specimens.

FIGURE 2: Tafel curves of the Group AR and Group Ti specimens.

3.1.2. DC Corrosion Tests. The potentiodynamic polarization curves (Tafel curves) were used to examine the electrochemical corrosion behaviour of the specimens. Figure 2 shows the Tafel curves of the Group AR and Group Ti specimens.

As illustrated in Figure 1, Group AR specimens showed higher corrosion potential and lower corrosion current density values than the Group Ti specimens.

TiO_2 coating (Group AR specimens) increased the corrosion potential and decreased the corrosion current density of the specimens.

3.1.3. Cyclic Polarization Test. Figure 3 shows the cyclic polarization curves of the Group AR and Group Ti specimens. As shown in Figure 3, Group AR specimen showed higher corrosion potential and lower corrosion current density values than the Group Ti specimen which means that the Group AR specimen has higher corrosion resistance than the Group Ti specimen. Cyclic polarization was used to qualitatively evaluate tendency to pitting (localized corrosion) in a corrosive environment. Hysteresis between forward and
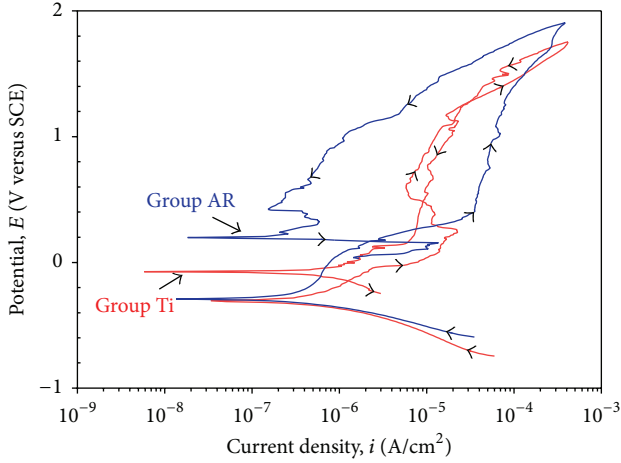
FIGURE 3: Cyclic polarization curves of the Group AR and Group Ti specimens.

TABLE 1: R_a (arithmetical mean roughness) and R_z (ten-point mean roughness) of the Groups Ti and AR determined by WLOP for $736 \times 480\ \mu m^2$ areas. Data are presented as the mean ± SD (standard deviation). Values are in micrometers (μm).

Groups	R_a (μm) ± SD	R_z (μm) ± SD
Ti	1.51 ± 0.02	12.76 ± 0.04
AR	4.08 ± 0.02	42.40 ± 0.27

reverse sweeps during cyclic polarization is an indication of pit formation. As shown in Figure 3, hysteresis (loop) was not observed in the Group AR and Group Ti specimens.

3.2. Surface Characterization

3.2.1. White Light Interference Microscopy. Quantitative roughness parameters R_a and R_z obtained from WLOP analysis for $1 \times 1.2\ mm^2$ areas for the Groups Ti and AR are shown in Table 1. Three-dimensional images of the surface topography of the Groups Ti and AR at ×5.1 magnification are shown in Figure 4. R_a and R_z surface roughness parameters values obtained from the Group AR quantitatively presented higher height descriptive parameters of roughness (Table 1).

3.2.2. Scanning Electron Microscopy. Figure 5 shows surface SEM images of sheets of cpTi (Group Ti) and the mixed-phase TiO$_2$ thin film photocatalyst (Group AR). It is observed that cpTi surface has a flat texture and showed relatively a smooth appearance. The surface morphology of the photocatalyst was affected by the electrochemical anodization. Craters (2–5 μm) and protruding hills (10–50 μm) were observed in Group AR anodized in the KOH electrolyte, conferring a more pronounced increase of surface roughness compared to cpTi sheets in Group Ti.

3.2.3. X-Ray Diffraction. The phase compositions of the obtained samples were characterized by XRD and the corresponding XRD patterns are shown in Figure 6. There was no

anatase or rutile diffraction peaks observed in cpTi surfaces in Group Ti. After anodization treatment and annealing at 550°C for 1 h, the mixed-phase composition of the Group AR was confirmed by its XRD patterns in Figure 6, where two sharp peaks located at the 2θ values of 38.4° and 27.4°, which are attributed to the diffraction of the (004) crystal plane of anatase TiO$_2$ and the (110) crystal plane of rutile phase TiO$_2$, respectively, indicating the crystallinity of the structure. Other characteristic peaks of the different crystalline phases are also marked on the pattern (Ti: titanium; A: anatase; R: rutile). Anatase and rutile contents (weight percentages) in each sample were confirmed by using Spurr-Myers' equations (see (1)) and the corresponding results of anatase and rutile were calculated as 54.6 wt% and 41.9 wt%, respectively.

3.3. Photocatalytic Activity Evaluation. The photocatalytic performance of anatase/rutile mixed-phase TiO$_2$ thin films in the degradation reaction of RhB dye solution was tested. Figure 7 shows the photocatalytic activity of both anatase/rutile mixed-phase TiO$_2$ thin films and cpTi surfaces under irradiation by UV light. The degradation of original RhB dye solution without photocatalyst was also plotted for comparison on glass as the control group. RhB dye concentration was decreased only by 4.4% and 2.4% (Group Ti and Group C, resp.) by the irradiation of ultraviolet for 120 min without the photocatalyst. This decomposition of RhB dye can be attributed to photolysis of RhB dye by ultraviolet. On the other hand, when the anatase/rutile mixed-phase TiO$_2$ thin films were used as photocatalyst, 22% RhB dye was degraded in 60 min, and the photocatalytical activity of RhB dye was maintained up to 26% in 120 min.

3.4. Colony-Forming Assay for Antibacterial Effect. UV irradiation had led to a significant decrease in the number of bacteria for all groups (Groups Ar and Ti: $p < 0.01$; Group D: $p < 0.05$). The number of bacteria decreased significantly in Group AR after 120 min of UV irradiation compared with all the other groups ($p < 0.01$) while bacteria were still detected after 120 min in all groups. In both UV (+) and UV (−) conditions no significant difference was found between the Groups Ti and D. Group AR showed statistically increased number of bacteria in UV (−) conditions (Groups Ti and D, $p < 0.01$) (Figure 8).

4. Discussion

The aim of this study was to develop antibacterial transmucosal components of dental implants less prone to peri-implantitis-associated bacteria colonization. This objective was achieved via surface modification by electrochemical anodization and annealing treatments. This study showed that anatase/rutile mixed-phase TiO$_2$ thin films inhibited adhesion of *A. actinomycetemcomitans*.

Based on previous studies, it is shown that surface roughness of the exposed transmucosal components is related with intraoral bacteria colonization over that surface [35]. In our subject, greater surface roughness can increase the total surface area, therefore creating more available active
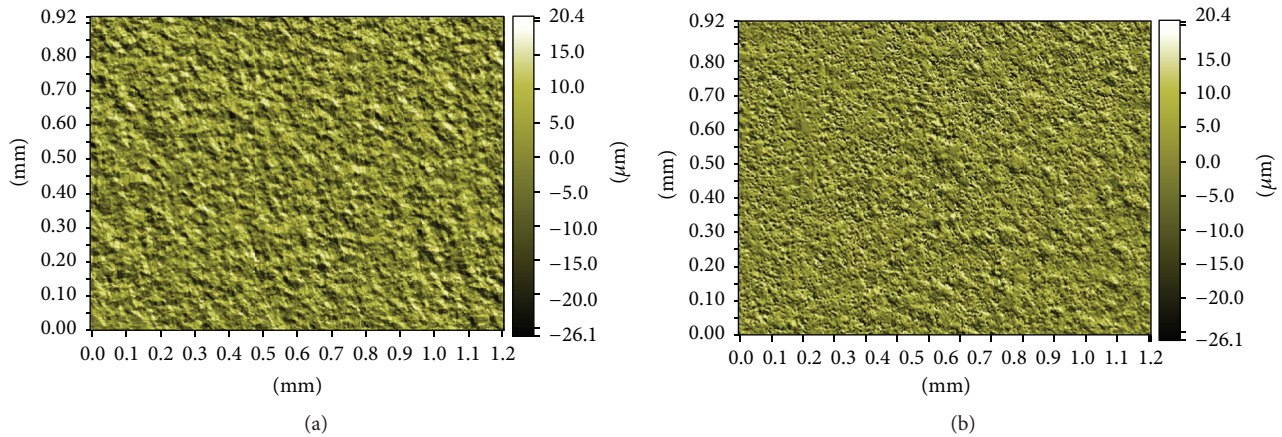
FIGURE 4: Representative WLOP images of (a) Group Ti, and (b) Group AR at ×5.1 magnification for 1×1.2 mm^2 areas.
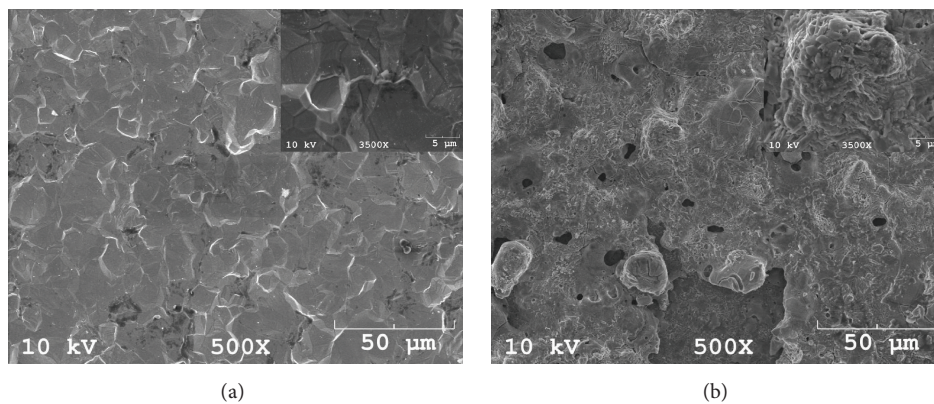

FIGURE 5: Representative top-view SEM micrographs of the (a) Group Ti, and (b) Group AR.

surface sites for reactions by higher photocatalytic reaction potential. By gaining a better understanding of the surface roughness and crystalline structure of different types of transmucosal dental implant components, practitioners will be better placed to utilize the most suitable part for any given prosthetic indication and to interpret the antibacterial clinical performance of these parts in relation to the patient needs and intraoral usage sites.

TiO$_2$ is usually used as a photocatalyst in two crystal structures: rutile and anatase. A postannealing is required to crystallize amorphous TiO$_2$ into anatase, rutile, or brookite structure [36]. In the present work, we aimed to form crystallized mixed-phase TiO$_2$ thin films consisting of anatase and rutile by annealing the electrochemically anodized sheets at 550°C after electrochemical anodization. Anatase/rutile mixed-phase TiO$_2$ thin films obtained by electrochemical anodization and annealing treatments were investigated by the photodegradation of RhB dye solution in order to prove photocatalytic activity. The rate of photodegradation was monitored by the decrease in the absorption value of the peak at 554 nm. Figure 7 shows the photodegradation efficiency of RhB dye solution as a function of UV irradiation time for the Groups Ti and AR as well as glass as control. The decrease in the absorption spectra of the dye solution

was monitored at regular intervals of time. Compared to the cpTi surfaces the anatase/rutile mixed-phase TiO$_2$ thin films exhibited photocatalytic efficiency. After two hours of irradiation under UV light, the RhB dye solution was degraded 26% by the anatase/rutile mixed-phase TiO$_2$ thin films. In order to elucidate and examine the above results, the crystallinity of the samples was detected by XRD and is shown in Figure 6 presenting several dominant peaks of anatase and rutile phase after annealing process. They indicated two sharp diffraction peaks at $2\theta = 38.4°$ and $27.4°$ that are identified to be (004) crystal plane of anatase TiO$_2$ and the (110) crystal plane of rutile phase TiO$_2$, respectively. Anatase and rutile contents (weight percentages) in each sample were calculated as 54.6 wt% and 41.9 wt%, respectively (Figure 6). Thus, electrochemical anodization treatment and annealing (550°C for 1 h) rendered a feasible and facile method to grow anatase and rutile phase TiO$_2$ from cpTi. This photocatalytic efficiency obtained from the anatase/rutile mixed-phase TiO$_2$ thin film containing about 54.6 wt% anatase phase and 41.9 wt% rutile phase was maintained up to 26% in 120 min. Our work illustrates that anatase/rutile mixed-phase TiO$_2$ thin films show higher photodegradation efficiency than the cpTi surfaces under UV in our run confirming enhanced photoactivity of cpTi titanium by electrochemical
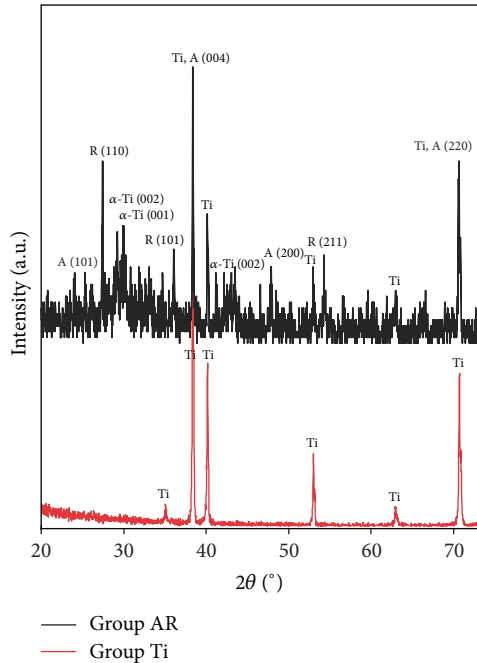
FIGURE 6: X-ray diffraction patterns of Group Ti: cpTi surface; Group AR: anatase/rutile mixed-phase TiO_2 thin film surface (Ti: titanium; A: anatase; R: rutile).
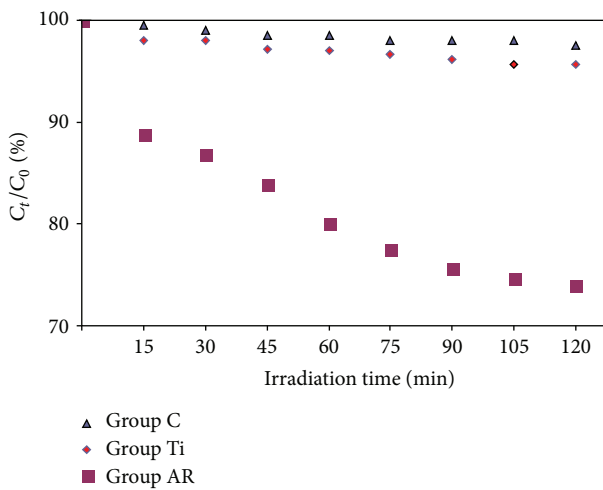

FIGURE 7: Photodegradation rate of RhB dye solution as a function of time under UV light irradiation on Group Ti: cpTi surface; Group AR: anatase/rutile mixed-phase TiO_2 thin film surface; Group C: glass surface.
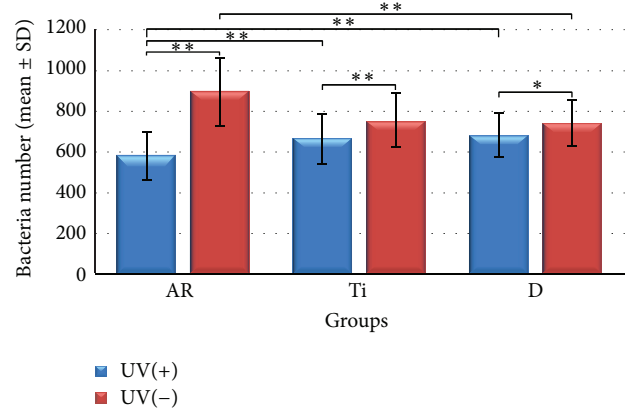

FIGURE 8: Descriptive analysis of adhesion of *A. Actinomycetemcomitans* on all groups tested (Group Ti: cpTi surface; Group AR: anatase/rutile mixed-phase TiO_2 thin film surface; Group D: culture plates' well bottoms). Data are presented as the mean ± SD ($n = 39$) for all bars. Results were analyzed using the two-way analysis of variance (ANOVA) followed by subsequent one-way ANOVA and Student's t-test. If one-way ANOVA suggested a significant difference between means among the groups, *post hoc* analyses were performed using Tukey HSD test, and Tamhane's $T2$ test (*$p < 0.05$, and **$p < 0.01$).

anodization and annealing treatments. This increase at the photocatalytical activity can be attributed to the difference in band gap energy of anatase and rutile structures of mixed TiO_2 films that were found to decrease the electron and hole recombination rate leading to an increase in the absorption of the surface organic species of the photocatalytic process [8]. Another explanation proposed by Hurum et al. (2003) is that, in mixed-phase TiO_2 under the presence of rutile crystals, charges produced on rutile by visible irradiation are stabilized through electron transfer to lower energy anatase lattice trapping sites at the transition points between these two phases [37]. Subsequent electron transfer moves the electron from anatase trapping sites to surface trapping sites, further separating the electron/hole pairs process [8]. The efficiency of photocatalysts is determined by recombination rates. Thus, rutile reduces the charge recombination rate of anatase and acts as an antenna to extend the photoactivity into visible wavelengths [37].

Electrochemical corrosion test results indicated that the passive oxide coating on the Ti specimens enhanced the corrosion resistance. Group AR specimens showed higher corrosion potential and lower corrosion current density than the Group Ti specimens, which was attributed to its protective passive oxide coating (Figures 1–3).

Photocatalytic TiO_2 coatings create contact-active surfaces that destroy the viability of the contacting microbes by photoenhanced formation of hydroxyl radicals [38]. This photocatalytic killing effect has been used in studies to eradicate bacteria around dental implants. Riley et al. (2005) considered if photoactive dental implants coated with nanostructured TiO_2 would eradicate *E. coli* when illuminated with UV light. The photoactivity of dental implants was established by photoenhanced decomposition of RhB dye solution. Irradiation of dental implants with UV light was found to be a suitable treatment for peri-implantitis [39]. In their study, photocatalytic activity was questioned to find a solution for peri-implantitis. But, the bacterium used was not intraoral bacterium which would not be expected to mimic the oral environment of a dental implant. Suketa et al. (2005) reported the bactericidal effect of the TiO_2 photocatalyst to be of great use for sterilizing the contaminated surface of dental implants. *Actinobacillus actinomycetemcomitans* and

Fusobacterium nucleatum were chosen for their study as these bacteria are responsible for the induction of inflammation of the gingivae, destruction of the periodontal ligament and alveolar bone associated with periodontal disease. The viability of both types of bacteria on the photocatalytic TiO_2 film was suppressed to less than 1% under UVA irradiation within 120 minutes [40]. Similarly, we chose *A. actinomycetemcomitans* for the colony-forming assay in our study has been implicated as it is the causative agent of several forms of severe periodontal disease [41]. UV irradiation had led to a significant decrease in the number of *A. actinomycetemcomitans* for all groups (Groups Ar and Ti: $p < 0.01$; Group D: $p < 0.05$) showing a killing effect of its own on all groups. Anatase/rutile mixed-phase TiO_2 thin films in Group AR significantly decreased the adhesion of *A. actinomycetemcomitans* after 120 min of UV irradiation compared with all the other groups ($p < 0.01$) showing a statistically significant photocatalytical killing effect in addition to the UV irradiation's killing effect. Antibacterial effect against *A. actinomycetemcomitans* on anatase/rutile mixed-phase TiO_2 thin films can be ascribed both to the UV irradiation and photocatalytical activity of Group AR containing crystal structures of anatase and rutile. But this combined killing effect was not able to kill all the bacteria on the surface of Group AR (Figure 8). In UV (−) conditions, Group AR showed statistically increased number of bacteria in UV (−) conditions (Groups Ti and D, $p < 0.01$) depending on its higher surface roughness values (Figure 4 and Table 1). cpTi surfaces in Group Ti were observed to be smooth and flat before electrochemical anodization (Figure 5(a)). Photocatalytically active anatase/rutile mixed-phase TiO_2 thin films with surface features of craters (2–5 μm) and protruding hills (10–50 μm) on Ti substrates (Figure 5(b)) were produced after electrochemical anodization. This enhancement in the bacteria number may be mainly attributed to the higher surface roughness of the anatase/rutile mixed-phase TiO_2 thin films allowing higher bacterial adhesion.

Photooxidation reaction of the terminal sulfhydryl group of CoA, which participates in many enzymatic reactions involved in the respiratory chain and fatty acid oxidations, is the reactive site of this molecule for the acyl transfer reactions and it is detrimental to cell viability. Nonselective actions of the highly oxidized species generated on the surface of the illuminated TiO_2 are expected to oxidize the cell membrane [42]. In this regard, a thorough understanding of the photocatalytical effect on the cell killing mechanisms of the human gingival soft tissues around dental implants should be questioned in addition to its suggested killing effect on oral bacteria around dental implants.

5. Conclusions

Anatase/rutile mixed-phase TiO_2 thin films fabricated by electrochemical anodization and annealing showed photocatalytic performance. The photocatalytic mechanism of TiO_2 film with mixed structure and the relationship between the contents of anatase with rutile phase brought forth antibacterial activity of these films which may further be considered for the antibacterial improvement applications for the transmucosal components of the dental implants. The findings, however, have to be verified in clinical settings.

Conflict of Interests

The authors declare that there is no conflict of interests regarding the publication of this paper.

Acknowledgments

References

[1] A. Fujishima and K. Honda, "Electrochemical photolysis of water at a semiconductor electrode," *Nature*, vol. 238, no. 5358, pp. 37–38, 1972.

[2] J. C. Yu, H. Y. Tang, J. Yu et al., "Bactericidal and photocatalytic activities of TiO_2 thin films prepared by sol-gel and reverse micelle methods," *Journal of Photochemistry and Photobiology A: Chemistry*, vol. 153, no. 1–3, pp. 211–219, 2002.

[3] T. Kawahara, Y. Konishi, H. Tada, N. Tohge, J. Nishii, and S. Ito, "A patterned TiO_2(anatase)/TiO_2(rutile) bilayer-type photocatalyst: effect of the anatase/rutile junction on the photocatalytic activity," *Angewandte Chemie*, vol. 41, no. 15, pp. 2811–2813, 2002.

[4] G. Rajagopal, S. Maruthamuthu, S. Mohanan, and N. Palaniswamy, "Biocidal effects of photocatalytic semiconductor TiO_2," *Colloids and Surfaces B: Biointerfaces*, vol. 51, no. 2, pp. 107–111, 2006.

[5] K. Maeda and K. Domen, "Photocatalytic water splitting: recent progress and future challenges," *Journal of Physical Chemistry Letters*, vol. 1, no. 18, pp. 2655–2661, 2010.

[6] P.-C. Maness, S. Smolinski, D. M. Blake, Z. Huang, E. J. Wolfrum, and W. A. Jacoby, "Bactericidal activity of photocatalytic TiO_2 reaction: toward an understanding of its killing mechanism," *Applied and Environmental Microbiology*, vol. 65, no. 9, pp. 4094–4098, 1999.

[7] M. R. Hoffmann, S. T. Martin, W. Choi, and D. W. Bahnemann, "Environmental applications of semiconductor photocatalysis," *Chemical Reviews*, vol. 95, no. 1, pp. 69–96, 1995.

[8] L. Zhao, M. Han, and J. Lian, "Photocatalytic activity of TiO_2 films with mixed anatase and rutile structures prepared by pulsed laser deposition," *Thin Solid Films*, vol. 516, no. 10, pp. 3394–3398, 2008.

[9] Y. R. Zhang and Q. Li, "Synthesis and characterization of Fe-doped TiO_2 films by electrophoretic method and its photocatalytic activity toward methyl orange," *Solid State Sciences*, vol. 16, pp. 16–20, 2013.

[10] A. Piscopo, D. Robert, and J. V. Weber, "Comparison between the reactivity of commercial and synthetic TiO_2 photocatalysts," *Journal of Photochemistry and Photobiology A: Chemistry*, vol. 139, no. 2-3, pp. 253–256, 2001.

[11] B. Kepenek, U. O. Seker, A. F. Çakır, M. Ürgen, and C. Tamerler, "Photocatalytic bactericidal effect of TiO_2 thin films produced

by cathodic arc deposition method," *Key Engineering Materials, Bioceramics 16*, vol. 254-256, pp. 463–466, 2004.

[12] J. Yu, X. Zhao, and Q. Zhao, "Photocatalytic activity of nanometer TiO_2 thin films prepared by the sol-gel method," *Materials Chemistry and Physics*, vol. 69, no. 1–3, pp. 25–29, 2001.

[13] K.-J. Shieh, M. Li, Y.-H. Lee, S.-D. Sheu, Y.-T. Liu, and Y.-C. Wang, "Antibacterial performance of photocatalyst thin film fabricated by defection effect in visible light," *Nanomedicine: Nanotechnology, Biology, and Medicine*, vol. 2, no. 2, pp. 121–126, 2006.

[14] D. Byun, Y. Jin, B. Kim, J. Kee Lee, and D. Park, "Photocatalytic TiO_2 deposition by chemical vapor deposition," *Journal of Hazardous Materials*, vol. 73, no. 2, pp. 199–206, 2000.

[15] K.-H. Wang, Y.-H. Hsieh, P.-W. Chao, and C.-Y. Cgang, "The photocatalytic degradation of trichloroethane by chemical vapor deposition method prepared titanium dioxide catalyst," *Journal of Hazardous Materials*, vol. 95, no. 1-2, pp. 161–174, 2002.

[16] M. Kemell, V. Pore, M. Ritala, M. Leskelä, and M. Lindén, "Atomic layer deposition in nanometer-level replication of cellulosic substances and preparation of photocatalytic TiO_2/cellulose composites," *Journal of the American Chemical Society*, vol. 127, no. 41, pp. 14178–14179, 2005.

[17] S. Mändl, R. Sader, G. Thorwarth et al., "Investigation on plasma immersion ion implantation treated medical implants," *Biomolecular Engineering*, vol. 19, no. 2–6, pp. 129–132, 2002.

[18] B. Kepenek, S. Öncel, A. F. Çakir, and M. Ürgen, "Photoactive TiO_2 coatings on metal substrates by cathodic arc deposition technique," *Key Engineering Materials*, vol. 264–268, pp. 549–552, 2004.

[19] K. Lee, D. Kim, P. Roy et al., "Anodic formation of thick anatase TiO_2 mesosponge layers for high-efficiency photocatalysis," *Journal of the American Chemical Society*, vol. 132, no. 5, pp. 1478–1479, 2010.

[20] J. C. Ireland, P. Klostermann, E. W. Rice, and R. M. Clark, "Inactivation of *Escherichia coli* by titanium dioxide photocatalytic oxidation," *Applied and Environmental Microbiology*, vol. 59, no. 5, pp. 1668–1670, 1993.

[21] B. Kim, D. Kim, D. Cho, and S. Cho, "Bactericidal effect of TiO_2 photocatalyst on selected food-borne pathogenic bacteria," *Chemosphere*, vol. 52, no. 1, pp. 277–281, 2003.

[22] S.-H. Lee, S. Pumprueg, B. Moudgil, and W. Sigmund, "Inactivation of bacterial endospores by photocatalytic nanocomposites," *Colloids and Surfaces B: Biointerfaces*, vol. 40, no. 2, pp. 93–98, 2005.

[23] P. Amézaga-Madrid, R. Silveyra-Morales, L. Córdoba-Fierro et al., "TEM evidence of ultrastructural alteration on *Pseudomonas aeruginosa* by photocatalytic TiO_2 thin films," *Journal of Photochemistry and Photobiology B: Biology*, vol. 70, no. 1, pp. 45–50, 2003.

[24] J. B. Kaplan, M. F. Meyenhofer, and D. H. Fine, "Biofilm growth and detachment of *Actinobacillus actinomycetemcomitans*," *Journal of Bacteriology*, vol. 185, no. 4, pp. 1399–1404, 2003.

[25] A. Prusi, L. Arsov, B. Haran, and B. N. Popov, "Anodic behavior of Ti in KOH solutions—Ellipsometric and micro-Raman spectroscopy studies," *Journal of the Electrochemical Society*, vol. 149, no. 11, pp. B491–B498, 2002.

[26] S. Sugapriya, R. Sriram, and S. Lakshmi, "Effect of annealing on TiO_2 nanoparticles," *Optik*, vol. 124, no. 21, pp. 4971–4975, 2013.

[27] D. Mareci, R. Chelariu, I. Dan, D.-M. Gordin, and T. Gloriant, "Corrosion behaviour of beta-Ti20Mo alloy in artificial saliva," *Journal of Materials Science: Materials in Medicine*, vol. 21, no. 11, pp. 2907–2913, 2010.

[28] Y. Oshida, C. B. Sellers, K. Mirza, and F. Farzin-Nia, "Corrosion of dental metallic materials by dental treatment agents," *Materials Science & Engineering C: Biomimetic and Supramolecular Systems*, vol. 25, no. 3, pp. 343–348, 2005.

[29] L. G. Devi, N. Kottam, and S. G. Kumar, "Preparation and characterization of Mn-doped titanates with a bicrystalline framework: correlation of the crystallite size with the synergistic effect on the photocatalytic activity," *Journal of Physical Chemistry C*, vol. 113, no. 35, pp. 15593–15601, 2009.

[30] X. Z. Fu, L. A. Clark, Q. Yang, and M. A. Anderson, "Enhanced photocatalytic performance of titania-based binary metal oxides: TiO_2/SiO_2 and TiO_2/ZrO_2," *Environmental Science & Technology*, vol. 30, no. 2, pp. 647–653, 1996.

[31] R. A. Spurr and H. Myers, "Quantitative analysis of anatase-rutile mixtures with an X-ray diffractometer," *Analytical Chemistry*, vol. 29, no. 5, pp. 760–762, 1957.

[32] S. K. Zheng, G. Xiang, T. M. Wang, F. Pan, C. Wang, and W. C. Hao, "Photocatalytic activity studies of TiO_2 thin films prepared by r.f. magnetron reactive sputtering," *Vacuum*, vol. 72, no. 1, pp. 79–84, 2003.

[33] S. Yeniyol, Z. He, B. Yüksel et al., "Antibacterial activity of As-annealed TiO_2 nanotubes doped with Ag nanoparticles against periodontal pathogens," *Bioinorganic Chemistry and Applications*, vol. 2014, Article ID 829496, 8 pages, 2014.

[34] W. D. Dupont and W. D. Plummer Jr., "Power and sample-size calculations—a review and computer-program," *Controlled Clinical Trials*, vol. 11, no. 2, pp. 116–128, 1990.

[35] R. Bürgers, T. Gerlach, S. Hahnel, F. Schwarz, G. Handel, and M. Gosau, "*In vivo* and *in vitro* biofilm formation on two different titanium implant surfaces," *Clinical Oral Implants Research*, vol. 21, no. 2, pp. 156–164, 2010.

[36] A. W. Tan, B. Pingguan-Murphy, R. Ahmad, and S. A. Akbar, "Review of titania nanotubes: fabrication and cellular response," *Ceramics International*, vol. 38, no. 6, pp. 4421–4435, 2012.

[37] D. C. Hurum, A. G. Agrios, K. A. Gray, T. Rajh, and M. C. Thurnauer, "Explaining the enhanced photocatalytic activity of Degussa P25 mixed-phase TiO_2 using EPR," *Journal of Physical Chemistry B*, vol. 107, no. 19, pp. 4545–4549, 2003.

[38] Y. Ohko, Y. Utsumi, C. Niwa et al., "Self-sterilizing and self-cleaning of silicone catheters coated with TiO_2 photocatalyst thin films: a preclinical work," *Journal of Biomedical Materials Research*, vol. 58, no. 1, pp. 97–101, 2001.

[39] D. J. Riley, V. Bavastrello, U. Covani, A. Barone, and C. Nicolini, "An in-vitro study of the sterilization of titanium dental implants using low intensity UV-radiation," *Dental Materials*, vol. 21, no. 8, pp. 756–760, 2005.

[40] N. Suketa, T. Sawase, H. Kitaura et al., "An antibacterial surface on dental implants, based on the photocatalytic bactericidal effect," *Clinical Implant Dentistry and Related Research*, vol. 7, no. 2, pp. 105–111, 2005.

[41] J. J. Zambon, L. A. Christersson, and J. Slots, "*Actinobacillus actinomycetemcomitans* in human periodontal disease: prevalence in patient groups and distribution of biotypes and serotypes within families," *Journal of Periodontology*, vol. 54, no. 12, pp. 707–711, 1983.

[42] D. M. Blake, P.-C. Maness, Z. Huang, E. J. Wolfrum, J. Huang, and W. A. Jacoby, "Application of the photocatalytic chemistry of titanium dioxide to disinfection and the killing of cancer cells," *Separation and Purification Methods*, vol. 28, no. 1, pp. 1–50, 1999.